Synthesis and Optimization of $Ni_xMn_{1-x}Fe_2O_4$ Catalyst in Chemical Looping Steam Methane Reforming Process

Nazari, Mousa; Heydarinasab, Amir*[+]

Department of Petroleum and Chemical Engineering, Science and Research Branch, Islamic Azad University, Tehran, I.R. IRAN

Soltanieh, Mohammad

Department of Chemical and Petroleum Engineering, Sharif University of Technology, Tehran, I.R. IRAN

Maddah, Bozorgmehr

Department of Chemistry, Faculty of Science, Imam Hossein University Tehran, I.R. IRAN

ABSTRACT: *The $Ni_xMn_{1-x}Fe_2O_4$ oxygen carrier is synthesized through the chemical precipitation method to be applied in the Chemical Looping Steam Methane Reforming (CL-SMR) process. The Response Surface Method (RSM) is adopted based on the Central Composite Design (CCD) model to evaluate the effect of the independent variables on the responses' functionality and to predict the best response volume. The variables: reaction temperature (550-750°C), Oxygen Carrier (OC) loading rate (0.1-0.9), steam per methane ratio (S/C) (1.5-3.5), oxidation-reduction cycles' count (1-9), and the responses consisting of CH_4 conversion percentage, CO/CO_2 molar ratio, and H_2 production yield are assessed. The analysis of variance (ANOVA) results indicates that reaction temperature and the OC type are the most effective, while the oxidation-reduction cycles' count is the least effective on CH_4 conversion percentage and H_2 production yield. By implementing the optimized results in laboratory conditions, it is revealed that the $Ni_{0.6}Mn_{0.4}Fe_2O_4$ OC at operating conditions at 650°C, S/C=2.5, and 9 redox cycles, the best response to the CH_4 conversion percentage, CO/CO_2 molar ratio, and, H_2 production yield with 99.6, 15.7, and 77.6, respectively. The improved stability and functionality of the OC reveal that during the 24 redox cycle the self-supported $Ni_{0.6}Mn_{0.4}Fe_2O_4$ OC is of high stability, high CH_4 conversion percentage means, and high H_2 production yield. The OCs samples are characterized by applying FT-IR, XRD, FESEM with X-ray spectroscopy EDX, BET, and TGA.*

Keywords: *Oxygen carrier; $Ni_xMn_{1-x}Fe_2O_4$ nano-powder; CL-SMR process; Response Surface Method; H_2 production.*

INTRODUCTION

The pollution caused by energy carriers is one of the important issues facing human life. Fossil fuels, natural gas in specific, are among the most essential fuel resources consumed in many industries in considerable volume.

***** *To whom correspondence should be addressed.*
+ *E-mail*: *a.heidarinasab@srbiau.ac.ir*
1021-9986/2021/5/1584-1606 23/$/7.03

Production of environmental pollutants including greenhouse gases and acidic gases like CO_2, CO, and SO_x is a major concern directly related to these fuels, consequently. The necessity for an alternative fuel resource is a growing issue. Many studies are run to assess alternative energy carriers. Hydrogen is a clean fuel and a new renewable energy resource that generates only steam during its combustion process and does not emit pollutants like greenhouse gases and acidic gases in the air is focused on. All hydrocarbon fuels can be applied as raw materials in H_2 production yield. A great part of the H_2 needed in industries is provided by H_2 fuels like natural gas [1, 2]. There exist different methods in producing H_2 from natural gas, among which the SMR method is the most common and economically feasible. This process is very complex and difficult because the absorption and storing of CO_2 are major concerns. Applying H_2 as an energy resource must be justifiable in an economic sense and must be capable of absorbing and storing the produced CO_2. The Chemical Looping (CL) technology for H_2 production is focused on due to its high H_2 purity and relying on more H_2 production without resorting to air or H_2 gas separation and CO_2 absorption units. In producing H_2 in the CL process, to oxidize CH_4 by lattice oxygen, the OC structure is applied instead of pure oxygen [1 and 3-6]. Consequently, the investment cost of H_2 plant construction is out of the question. One of the basic issues in these processes is the selection of an appropriate OC, which should have a high conversion percentage, selectivity to the intended material, resistance against heat or thermal shock, high resistance against agglomeration, ability to circulate in multiple redox systems, trivial carbon precipitation, low production cost while being environment-friendly [6-8]. Many studies are run on the iron-based OC due to its features like being environmentally friendly, having strong catalyst activity, and relatively low production cost with other metal-based carriers like that of Co, Ni, Cu, and Mn in CH_4 reforming processes. Iron oxide has different oxide states with reduction degrees of hematite to magnetite ($Fe_2O_3 \rightarrow Fe_3O_4$) reduction with a high velocity leading to the conversion of CO and H_2 to CO_2 and H_2O, respectively, and the stages including magnetite to ferrous oxide reduction ($Fe_3O_4 \rightarrow FeO$) and ferrous oxide to iron ($FeO \rightarrow Fe$) with a very low velocity where due to balance limitations, are of low conversion percentage. The Fe_2O_3 iron oxide is of low reactivity with other metal-based OCs like CuO and NiO. Consequently, by considering the limitation due to established thermodynamic balance, the second stage of reducing magnetite to ferrous oxide and ferrous oxide to iron would be appropriate for CLR [8 -16]. Metal oxides lead to a reduction in CO_2 capacity, among which iron oxide has the highest CO_2 reduction capacity, but due to agglomeration on its surface, this metal becomes inactive in a rapid manner. Combining different materials with metal oxide prevents the generation of Sintering effects and contributes to its reactivity and appropriate selectivity. Hence, the combined metal oxide may be a candid OC alternative, due to its better reactivity and renewability [17]. Depending on the partial pressure of oxygen, the spinel ferrites with A-Fe_2O_4 general formula, where, A= Cu, Mn, Mg, Ni, and Co can replace the available Oxygen vacuum in their structure with Oxygen at high temperatures [18].

Adding supportive material to the iron-based OC leads to a reduction in oxygen transference (RO) capacity and affects the thermodynamic reduction thereof. Applying supportive materials to prevent the Fe_2O_3 OC Sintering is essential. Some supportive materials like Al_2O_3 and TiO_2 are capable to react to FeO, leading to the complete oxidation of H_2 and CO and producing $FeAl_2O_3$ and $FeTiO_3$, respectively [8]. The concept of applying supportive materials like the iron-based OC in CL is assessed to a great extent in [17,18].

The combined metal oxides of ferrite type have great catalyst functionality due to their specific crystalline structure [10, 17, 19-27]. Through the H_2 chemical looping (CLH) process the $NiFe_2O_4$ and $CoFe_2O_4$ spinel ferrites are applied as OCs to produce H_2 and CO_2, where it is revealed that subject to similar conditions of oxidation and reduction, through the $NiFe_2O_4$ and $CoFe_2O_4$ OC, the total H_2 production volume becomes four-fold higher than that of the Fe_2O_3 OC and the CH_4 conversion yield is 100% and 22% for spinel ferrites and Fe_2O_3, respectively, that is, the combined metal ferrites are of higher capability in producing H_2 [19].

The $A-Fe_2O_4$ (A= Mn, Zn, Cu, Co, and Ni) spinel ferrites are synthesized as OCs in the Chemical Looping Combustion (CLC) process through the conventional ceramic technology of solid-state reaction method. These spinel ferrites are evaluated in a fixed-bed reactor in 5-10 oxidation-reduction cycles. It is revealed that these spinel ferrites are capable of transferring the lattice oxygen

to the fuel in the reduction stage and obtain their lattice oxygen in the presence of air in the oxidation stage. The Cu, Co, and Ni ferrites are of a higher capability to transfer lattice oxygen with Mn ferrites. The Cu ferrites are very active with the maximum CH_4 conversion percentage >95%, while the opposite holds in the case of the Mn ferrite, about 30%. The Co ferrites have considerable sustainability in consecutive cycles, with CH_4 conversion of 68%. The Zn and Ni ferrites are of high CH_4 conversion degree in different redox cycles, that is, 90% and 78%, respectively, [18].

To apply an appropriate OC in the CLR process, the Co, Cu, Mn, and Fe OCs are synthesized subject to Al_2O_3 support through the precipitation method, and next, the variables consisting of reaction temperature (700 to 1050°C), reaction time (10 to 70 min) and carrier type (iron, manganese, cobalt, and copper with aluminum support) and the responses consisting of H_2 production yield, CH_4 conversion and, CO_2 selectivity are assessed through the CCD method. The ANOVA results indicate that the OC type has the highest effect on all the results. Iron has the highest resistance in relation to precipitation formation compared to these four OCs. The optimization results indicate that the best response for the iron-based OC subject to 1014.13°C temperature is 55.5 min reaction time, where the H_2 production yield, CH_4 conversion, and CO_2 selectivity are 83.45, 79.09, and 2.26, respectively [9].

The reactivity of iron oxide and nickel on the Chemical Looping Dry Reforming (CLDR) process is assessed, where it is revealed that the iron can be converted into the Fe_2O_4 oxide subject to CO_2, but not a nickel. The oxidation capability of Fe_2O_3 is < mixed oxides $NiO-Fe_2O_3$ < Synthesized $NiFe_2O_4$ <NiO, while the reduction capability of NiO <Fe_2O_3< mixed oxides $NiO-Fe_2O_3$ < Synthesized $NiFe_2O_4$, because the effects of the nickel and iron cooperation and the formation of the spinel structure thereof, makes the redox capability synthesized $NiFe_2O_4$ higher than that of the $NiO-Fe_2O_3$ combined oxide [13]. Oxygen-free ferrite and the completely reduced $NiFe_2O_4$ products can improve the lattice oxygen through CO_2 oxidation. Oxygen-free ferrite can cause CO_2 reduction to a great extent. Hence, the nickel ferrite is applied as an OC in H_2 production which can have a good reaction in the oxidation-reduction consecutive process through the CL [17]. Every metal oxide combination due to its positive effect allows its appropriate application, which in turn increases the OC functionality. The spinel structures together with metal elements expose good reactions. The combination of some metal elements is beneficial in enhancing the redox capability in iron-containing OC, that is, adding Ni and Mn in the OC can provide positive effects in the CL-SMR process. To the authors' best knowledge; there exists no study on the spinel structures containing some metal oxides in the CL-SMR process, though it is well known that the assessment and identification of catalysts' functionalities containing different metal elements is a complex task. It is notable that the available studies with the objective of applying OCs in the CL-SMR process are run in a four staged reactor which is not capable of providing all the operational conditions together with the interactions within the functional parameters. To run these studies many experiments are necessary which in turn may require too much time, cost, and material [17, 21, 28-32]. To overcome this drawback the experiments were designed by adopting the Response Surface Method (RSM), whereby modeling and optimizing the reaction variables through statistical methods, the question of how do the factors affect the process can be assessed [33].

By combining several metal oxides, the positive effect of each can be applied appropriately. This kind of compound increases OCs functionality. The same is advantageous in increasing the redox capability in oxidation-containing iron. Combining metals like Mn, Ni, Cu, and Mg in OCs with spinel structure can have positive effects on the CL-SMR process. The contribution of the metal element in the mixed metal ferrites (Mn, Ni, Zn, Co, Cu, Mg, etc.) in H_2O decomposing and producing H_2 in the CL-SMR process is not well realized and needs further assessments.

The objective of this study is to synthesis the OC of spinel structures containing different metal oxides and assess these OCs' functionality in a quartz fixed-bed micro-reactor for the CL-SMR process. The experiments are designed through the RSM to optimize the parameters affecting the CL-SMR process subject to different functionalities. There exists no study on the multi-metal spinel to be applied in the CL-SMR process together with the optimization of the variables and parameters affecting the same.

EXPERIMENTAL SECTION

OC Preparation

To synthesize the $Ni_xMn_{1-x}Fe_2O_4$ OC at the nm scale, the chemical precipitation method is adopted. The materials

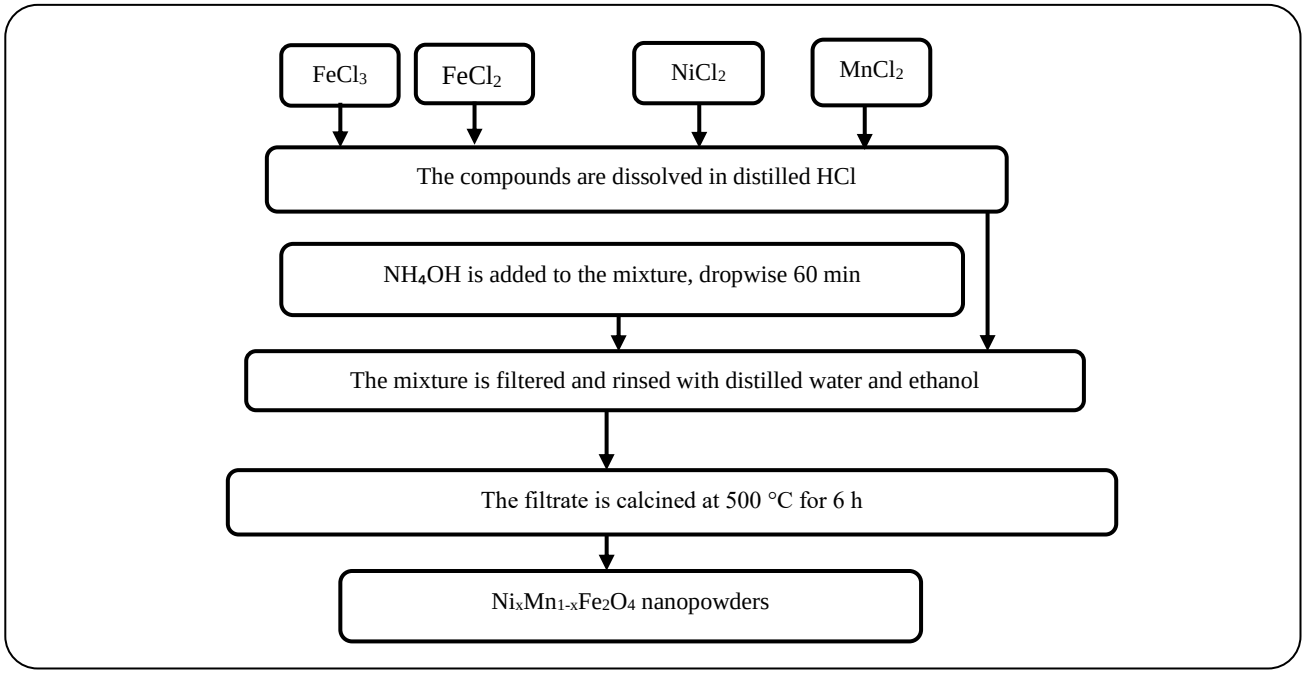

Fig. 1: OCs synthesis process flowchart.

applied in synthesizing these combinations consist of ammonia of 25% purity, iron II chloride, hydrochloric acid (25% purity), ethanol, $NiCl_2.6H_2O$ and, $MnCl_2.4H_2O$ all purchased from Merck Co with high purities.

To begin with, first, 1 molar HCl solution is provided through which the, $NiCl_2.6H_2O$, $MnCl_2.4H_2O$, and iron chloride II solutions are converted into 0.5, 0.5, and 1 M, respectively. The intended solutions are combined per stoichiometry ratio for 15 min at room temperature and stirred in a magnetic mixer to which the 2 M ammonia is added in droplets until PH >8 is yielded. At this stage, first, two liters of distilled water is added to this brownish mix and the container is placed in a strong and big magnet for 15 min to allow the OC particles' deposition, and next, the water is removed. This rinsing operation is repeated three times, followed by filtering the deposit and rinsing it with ethanol to remove the impure organic materials. The final deposit is dried for 8 h at 70°C and calcined for 6 h at 500°C.

To assess the quality of different molecules, determining the molecule structure of different species, the organic in specific, and identifying the available function groups in the synthesized OC structures, is accomplished by applying the Bruker Tensor 27 FT-IR within 400 to 4000 cm^{-1} range with 4 cm^{-1} clarity range. To assess the materials' structures, the XRD pattern is applied through the Philips, X, pert-MPD device with Cu Kα X-Ray wavelength of 1.54 A° with an angular speed of 2°C/min of 20°-80°. The morphologic analysis of nanostructures, particle sizes, and chemical combinations identification of OC are run through the FE-SEM QUANTA 200 apparatus equipped with Energy-Dispersive X-ray (EDX) spectroscopy (EDAX EDS Silicon DRIFT 2017) device. The porosity and the specific surface area of the OCs are obtained by adopting the BET method (Belsorp mini II model Bell). The ThermoGravimetric Analyses (TGA) of the OCs are run on an STA-504 thermal analyzer with a 10°C/min (from 30 to 800°C), heating rate, and 25 mL/min airflow. This analysis is a flowchart in Fig. 1. the chemical reaction of this OC is expressed as follows:

$$xNiCl_2+(1-x)MnCl_2+2FeCl_2+yNH_4OH+H_2O\rightarrow$$
$$Ni_{(x)}Mn_{(1-x)}Fe_2O_4+(y-8)NH_4OH+8NaCl+5H_2O$$

Experimental reactor and procedure

To evaluate the synthesized OCs' activity and selectivity, for both the oxidation-reduction processes in the SMR, a fixed-bed quartz reactor of 400 mm length with a 12 mm internal diameter is applied. This reactor is placed in a cylindrical furnace where the temperature is adjusted through a K-type thermocouple placed in the reactor center. The flows entering the reactor consist of methane,

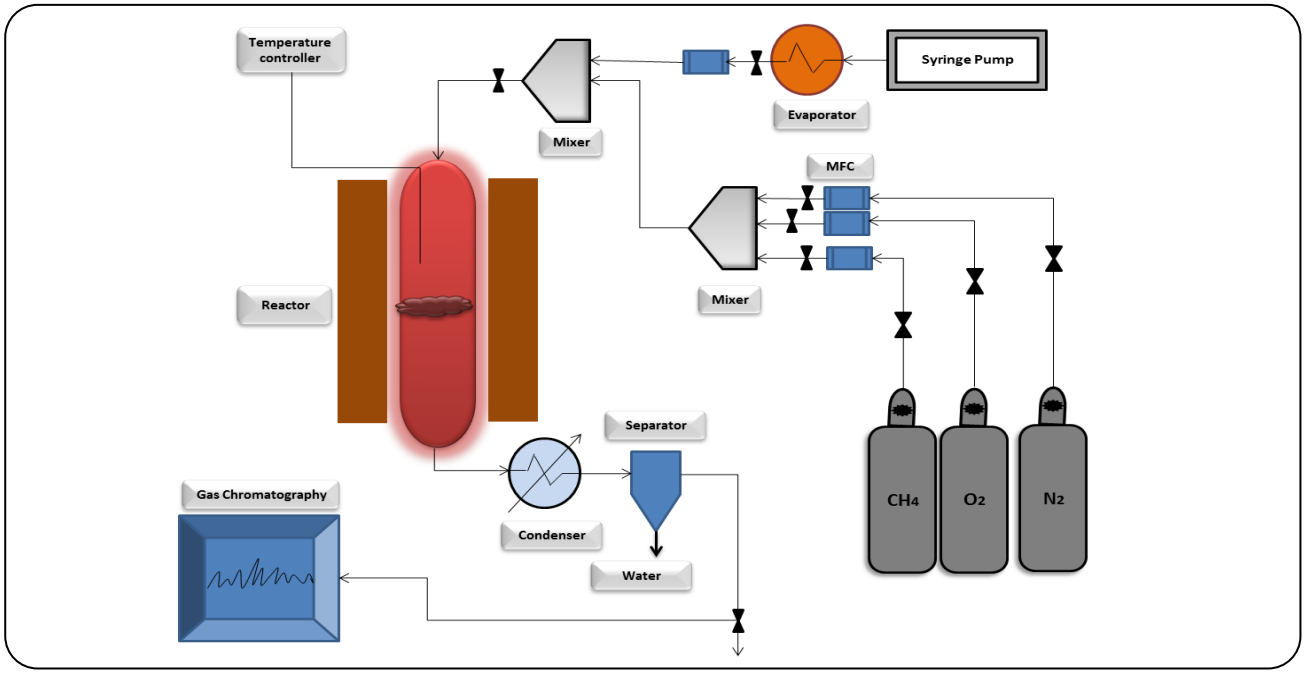

Fig. 2: Reactor system of CL-SMR process

nitrogen, and oxygen gas types each with 99.99% purity and the same for steam. Their flow intensity is measured through the gas flow intensity (MFC) at high accuracy, to provide the necessary steam. In this process, the distilled water enters the electric furnace through a laboratory syringe pump to become water steam and then enter the reactor together with gas. After the reforming reaction, the exiting flows are cooled through a condenser, and the produced gas is evaluated through the Shimadzu 4C-TPC gas chromatograph equipped with thermal conductivity and flame ionization detectors. The schematic of this reactor system is presented in Fig. 2.

Here, an experiment was run with an emphasis on SMR and its oxidation process with air. Where 2.5 g OC of 150 to 200 μ mesh size is placed at an appropriate condition of the reactor by dominant contact with gas and prevention of any side effects. By adjusting the reactor temperature to 600 °C and assuring the complete oxidation of the catalysts before running the experiment, the following two operational conditions are evident:

To run the SMR in the reduction cycle, the reactor was fed with reactive gas' flow containing 50 mL/min CH_4 and 150 mL/min steam (S/C=3) through a 100 mL/min non-effective N_2 gas within 40 min in a parallel manner. As to the oxidation cycle, the reactive gases flow route at the reduction cycle becomes closed 20% oxygen gas mixture together with the N_2 sweep gas at 150 mL/min was injected into the reactor in 20 min. In each redox cycle, 100 mL pure N_2 gas was injected into the reactor for 3 min to make all the remaining gases in the reactor to exit the reactor. The reactor system specifications and experiment instructions are tabulated in Table 1. The CH_4 conversion percentage, H_2 production yield, and molar ratio of CO/CO_2 are obtained through Eqs. (1, 2, and 3), respectively:

$$X_{CH_4} = \frac{(\text{moles of } CH_4)_{in} - (\text{moles of } CH_4)_{out}}{(\text{moles of } CH_4)_{in}} \times 100 \quad (1)$$

$$H2Yield(\%) = \frac{\text{moles of } H_2 \text{ produced}}{2(\text{total moles of } CH_4 + \text{feed}) + (\text{total moles of } H_2O + \text{feed})} \times 100 \quad (2)$$

$$CO/CO_2 \text{ molar ratio} = \frac{\text{moles of CO}}{\text{moles of } CO_2} \times 100 \quad (3)$$

RESULTS AND DISCUSSION

OC characterization

The XRD pattern of the $Ni_xMn_{1-x}Fe_2O_4$ (with x=0.1, 0.3, 0.4, 0.5, 0.7, and 0.9) nanoparticles' synthesis is illustrated in Fig. 3. Where the different 2θ= (30.6, 35.6,

Table 1: Specifications of the reactor system and the experimental procedure in a CL-SMR process.

Catalyst specification	Gas flow rate			Reactor system	
Height Diameter Temperature Pressure	400 mm 12mm 500- 750 °C Ambient	N_2 CH_4 O_2 Steam	99.99% purity 99.99% purity 99.99% purity Distilled water	Particle size Mesh size Catalyst weight	100 nm ≤ 150–200µ 2.5 g
Experimental stage	Gas flow rate (mL/min)		Time reaction (min)	Factor	
Sweep gas Reduction Oxidation	N_2 Steam / CH_4 and N_2 20% O_2 and 80 % N_2		3 40 20	100 150 / 50 and 100 150	

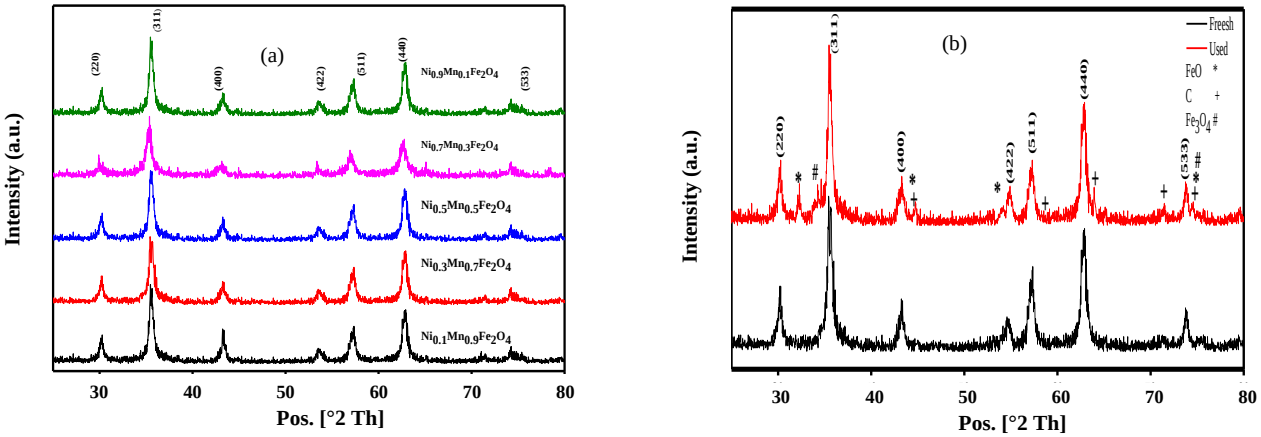

Fig. 3: XRD patterns of (a) fresh $Ni_xMn_{1-x}Fe_2O_4$ (x=0.1, 0.3, 0.5, 0.7, and 0.9) OCs and (b) fresh and second-hand $Ni_{0.6}Mn_{0.4}Fe_2O_4$ OCs.

43.3, 53.7, 56.1, 63.3, and 74.5) crystal plates corresponding to (220), (311), (400), (422), (511), (440), and (533) plates, respectively are observed. The position and intensity of all the peaks generated from this range correspond to that of the JCPDS cards (# 380430 for $MnFe_2O_4$ and # 742081 for $NiFe_2O_4$) standard peak [34,35]. No extra peak is observed in this pattern, indicating that there exist no impurities in the provided samples. The nanoparticles' mean (D) of crystal dimensions $Ni_xMn_{1-x}Fe_2O_4$ is obtained through the following Debye-Scherrer equation [36]:

$$D = \frac{0.89\lambda}{\beta \cos\theta_0} \quad (4)$$

Where D is the crystal dimension (nm), λ is the wavelength at 0.154 nm, β is the peak width at half-width maximum, and θ_0 is the Bragg diffraction angle. The average crystal size of $Ni_xMn_{1-x}Fe_2O_4$ powder was estimated by XRD about 20-50 nm.

The FT-IR analysis is run on the sample prepared by 0.2 mg $Ni_xMn_{1-x}Fe_2O_4$ (x=0.1, 0.3, 0.4, 0.5, 0.7, and 0.9) powder mixed with 200 mg KBr powder to determine purity and identify the OC production phase. The FT-IR of these nanoparticles within 400-4000 cm^{-1} range is illustrated in Fig. 4.

The peaks absorbed within the 450-900 cm^{-1} range correspond to that of the metal oxides (M-O). The strong absorption peaks appearing within the 3170-3600 cm^{-1} range correspond to that of the hydroxide (O-H) group. The 1629 cm^{-1} peak corresponds to the (O-H) water group (H_2O), indicating absorbed water on the ferrite spinel materials' surface. The very fine peak at 2362 cm^{-1} relates to CO_2 available in the air. According to the results obtained from the FT-IR range, it is revealed that no effect is caused by the existence of chloride and ammonium

Table 2: Physical characteristics of the fresh OCs.

Sample	D_{XRD} (nm)	S_{BET} (m^2/g)	Vp (cm^3/g)	dp (nm)
$Ni_{0.9}Mn_{0.1}Fe_2O_4$ (fresh)	28	5.02	0.016	9.28
$Ni_{0.7}Mn_{0.3}Fe_2O_4$ (fresh)	32	5.41	0.014	11.19
$Ni_{0.5}Mn_{0.5}Fe_2O_4$ (fresh)	31	6.37	0.018	13.4
$Ni_{0.3}Mn_{0.7}Fe_2O_4$ (fresh)	38	6.39	0.015	13.73
$Ni_{0.1}Mn_{0.9}Fe_2O_4$ (fresh)	43	5.37	0.019	14.39

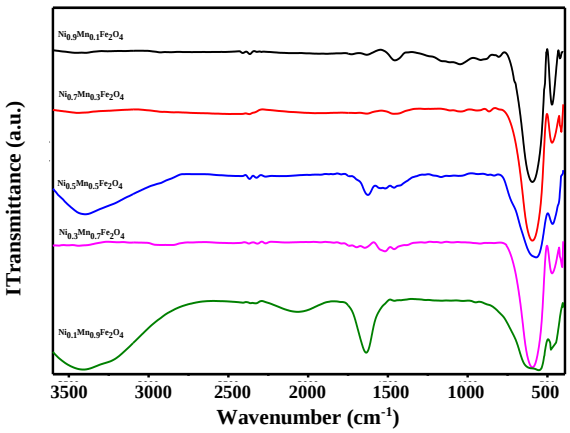

Fig. 4: FT-IR spectrum yield synthesized from OCs through the chemical precipitation method.

group impurities, indicating the synthesis of pure $Ni_xMn_{1-x}Fe_2O_4$ nano-powder [34, 37, 38].

Analyzing the specific surface area of OC is one of the essential parameters in determining the catalyst's functionality, [17, 39], for identifying the micro-structures particle through the BET test. In this test, the N_2 adsorption-desorption on OC particle surface is applied where the diameter, particle specific surface, volume, and pore size distribution are calculated through Barrett-Joyner-Halenda (BJH). For this purpose, BELSORP- mini II apparatus, BEL Japan was applied to determine the physical characteristics and OC particles' surface properties. To run the BET test, the OC is held for 2 hours at 250°C to allow the evaporation of possible steam in CO_2 and other molecules which might increase the pore volume, and then the sample is exposed to liquid nitrogen at -195.79°C followed by assessing the OC surface absorption and adsorption functionality. The physical properties of the synthesized OC $Ni_xMn_{1-x}Fe_2O_4$ (X= 0.1, 0.3, 0.5, 0.7, and 0.9) are tabulated in Table 2, and the pore size distribution is plotted in Fig. (5). The N_2 adsorption-desorption based on (IUPAC) categorization are of four classes [40]. Where, according to the synthesized OC it is revealed that the isotherm curve is of H3 type and pore size is of type II, indicating that these OCs are of mesopore structure. The results obtained from the BET test indicate that adding Mn to the OC structure would increase the specific surface area and the total catalyst pore volume. While this pattern is not always ascending and in continuation it follows a descending pattern which might possibly be due to pore blockage as to the high Mn weight percentage. The results obtained from BET and BJH have good correspondence with that of the XRD spectrum, indicating that an increase in Mn cannot always have a positive effect on the specific surface area and the total catalyst pore volume.

Experiment design and data analysis

Assessment of the most important operational variables is of concern in this design, where, determining their effect and interaction, together with simultaneously optimizing their volumes is inevitable. Running such experiments is more economically feasible and less time-consuming and provides better insights into the process of assessing the effect of each variable independently.

The RSM consists of mathematical and statistical techniques applied in developing and optimizing the processes where the intended response is affected by some variables, to define the correlation between the response and the variables for response optimization. The model applied in the RSM is the second-grade equation. A multi-sentence second-grade model is appropriate to establish a mathematical correlation between the response and the factors for four factors five-level design, Eq. (5):

$$Y = \beta_0 + \sum_{i=1}^{k}\beta_i X_i + \sum\sum_{i<j}\beta_i X_i X_j + \sum_{i=1}^{k}\beta_{ii} X_i^2 + \varepsilon \qquad (5)$$

Where Y is the response, X_i and Xj are the independent variables, β_0 is the constant coefficient, β_i, β_{ij}, and β_{ii} are the linear coefficients, the parameters' interaction

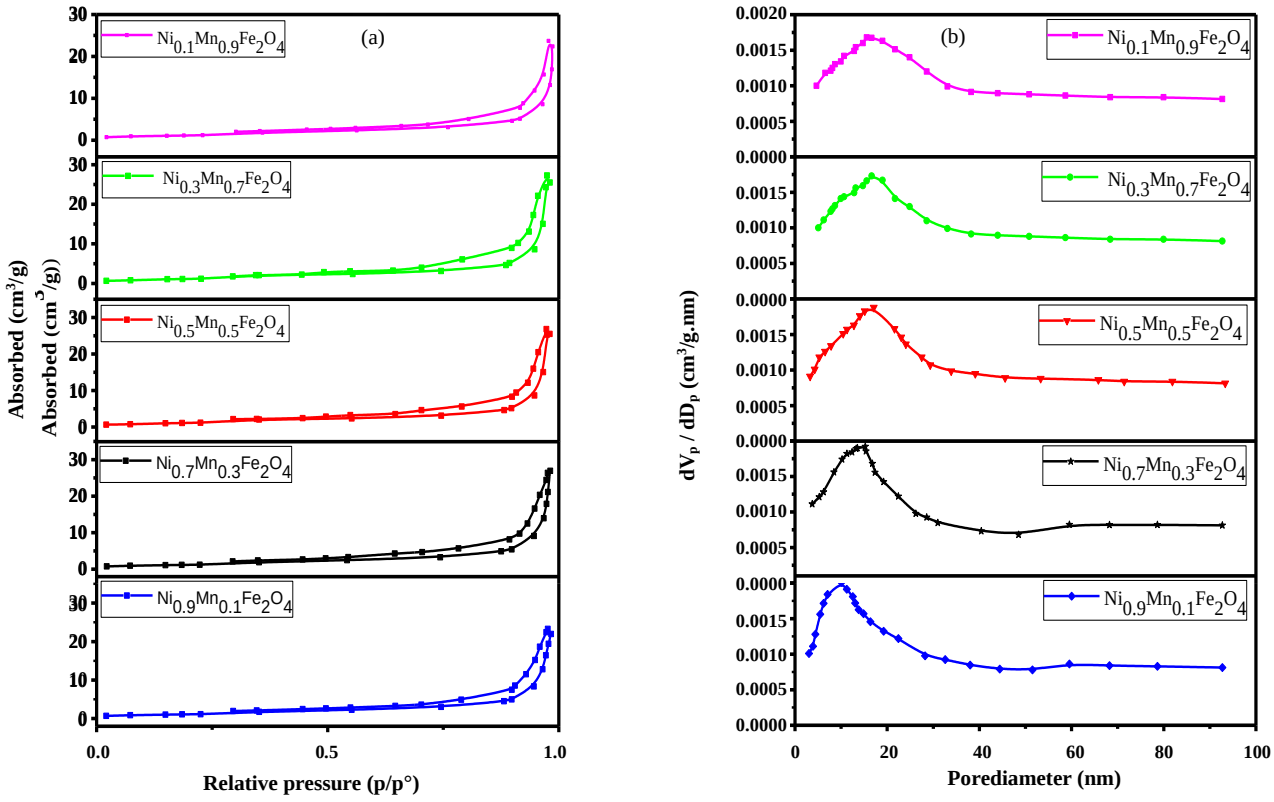

Fig. 5: a) N_2 adsorption-desorption isotherms distribution of fresh OCs and b) pore size distribution of fresh OCs.

coefficients and the quadratic coefficients, respectively, and ε is the model error [33, 41, 42].

By analyzing the obtained results and comparing them with the predicted results of the RSM, the correspondence between these two is assessed at a confidence level >95%. To evaluate the significant effects of the independent variables on the response variable, ANOVA is applied.

According to the primary experiments and the studies run by [9, 40, 43], the four factors of reaction temperature, OC loading rate, S/C ratio, and the oxidation-reduction cycles constitute the most important operational variables in the CL-SMR process, where the CH_4 conversion percentage, CO/CO_2 molar ratio, and H_2 production yield constitute the responses therein.

Here, the RSM based on the CCD is adopted to evaluate the effect of the independent variables on the response function and to predict the best response. In this design method, through the primary experiments and the authors' experiences, first, every variable's change range is determined, and next, based on the determining factors' interaction, five change levels are considered for every factor. Each variable level consists of one real volume and some dimensionless codified volumes. The codified levels of each variable consist of +1, -1, +α and –α. In this design, the variables' count (k) is 4 and α volume is 2, obtained through Eq. (6):

$$\alpha = 2^{k/4} \tag{6}$$

The designed experiment count is obtained through Eq. (7):

$$N = k^2 + (2 + k) + c_p \tag{7}$$

Where k is the count of the variables and C_p is the count of the iterations in the central point.

In this experimental design, the four factors of reaction temperature, OC loading rate, S/C ratio, and redox cycle count are considered at four iterations in the central point, where, according to Eq. (7), 28 experiments are proposed [40, 43]. The experiments' variables consist of different top and bottom axial levels (+α and -α), at the central level (0) and top and bottom levels (+1 and -1), the responses of which are designed through Design Expert S/W, Table 3. The proposed experiments and their responses are tabulated in Table 4. In this statistical model, the experiments are run randomLy based on statistical principles.

Table 3: The experiments' range and the independent variables' surfaces and the responses thereof

Factor	Name	Units	Minimum	Maximum	Coded Low	Coded High		Mean
A	Temp		500	700	-1 ↔ 550	+1 ↔ 650		600
B	Catalyst	°C	0.10	0.9	-1 ↔ 0.3	+1 ↔ 0.7		0.5
C	Cycle	%	1	9	-1 ↔ 1	+1 ↔ 9		5
D	S/C		1.5	3.5	-1 ↔ 2	+1 ↔ 3		2.5
Response	Name	Units	Observations	Minimum	Maximum	Mean	Std.Dev.	Model
R1	CH_4	%	28	65.3	100	91.33	8.94	Quadratic
R2	CO/CO_2		28	12.2	16.7	14.08	1.23	Quadratic
R3	H2	%	28	47.5	80.5	70.32	8.81	Quadratic

Table 4: The proposed experiments based on the CCD model together with their responses' real values.

Run	Factors				Responses			
	Temperature	Catalyst	Cycle	S/C	CH_4 %	CO/CO_2	H_2 %	CO
1	600	0.5	5	2.5	97.5	15.4	74.5	20.2
2	650	0.3	3	2	97.5	13.7	79.7	15.4
3	550	0.3	3	2	81.2	12.4	63.7	14.0
4	600	0.1	5	2.5	93.3	14.46	70.5	19.8
5	600	0.5	5	1.5	94.3	12.2	66.9	23.3
6	550	0.3	7	2	80.3	12.5	61.5	15.6
7	650	0.3	7	2	97.6	13.8	76.6	18.2
8	550	0.7	7	3	83.5	15.35	58.8	21.3
9	600	0.5	5	2	98.3	15.4	74.4	20.9
10	550	0.3	7	3	78.9	14.9	65.3	15.2
11	650	0.7	7	3	97.2	16.2	78.8	16.2
12	550	0.7	3	2	82.9	14	58.2	21
13	550	0.7	7	2	84.9	13.6	57.8	22.9
14	550	0.3	3	3	78.4	14.8	64.7	15.2
15	600	0.5	5	2.5	96.2	15.2	71.4	21.3
16	650	0.3	3	3	98.4	16.3	79.6	16.6
17	600	0.5	5	3.5	93.2	16.7	73.4	17.5
18	600	0.9	5	2.5	94.6	15.4	69.3	22.1
19	600	0.5	9	2.5	95.8	15.2	71	21.7
20	550	0.7	3	3	84.7	15.3	57.9	23.1
21	650	0.7	3	3	97.6	16.2	79.3	16.2
22	600	0.5	5	2.5	98.3	15.45	74.3	21.16
23	650	0.3	7	3	98.2	16.4	79.5	16.5
24	600	0.5	1	2.5	99.5	15.1	76.9	19.9
25	500	0.5	5	2.5	65.3	13.9	47.5	14.4
26	650	0.7	7	2	99.8	14.2	78.2	18.8
27	700	0.5	5	2.5	99.7	16.2	80.5	17.0
28	650	0.7	3	2	99.3	14.2	78.8	17.8

Statistical analysis

To economize time and cost in running the experiments with the possibility of assessing the effect of the variables and their interaction simultaneously, the assessment of the mentioned four factors on the reaction responses consisting of CH_4 conversion rate, CO/CO_2 molar ratio, and H_2 production yield is run through CCD, and ANOVA is applied for statistical analysis of responses. The initial statistical parameters selected and assessed to run the model consist of the mean, SD, coefficients of variation, R-squared (R^2) coefficient, and R^2 adjusted (Adj-R^2). The P-value ≤ 0.05 is the statistically significant level [9, 33, 42].

Evaluating the statistical models proposed for the responses

As to the CH_4 conversion percentage in the statistical model, the complete data are reported in their quadratic sense. The results obtained by evaluating the statistical model proposed for the responses are tabulated in Table 5. To estimate the validity of the obtained model, both the P and F-values are applied, as the lower and the higher parameters, respectively, the effectiveness of the given parameter on the model would be higher. According to the experiment design principles, P-value is a criterion in identifying the effect of each parameter level on the process response, that is, if the parameter P-value > 0.05, it has little or no effect and the process response making the response independent of this parameter [9, 33, and 42]. The statistical model proposed here is for the quadratic responses where the F-value for CH_4 conversion percentage, CO/CO_2 molar ratio and H_2 production yield is 110.23, 91.85, and 125.73, respectively, indicating a considerable model strength.

The experimental data with the volumes predicted for the different responses by the model are compared according to the ANOVA Table. The R^2 of CH_4 conversion percentage, CO/CO_2 molar ratio and H_2 production yield are 0.9789, 0.9818, and 0.9815, respectively. The R^2 volume varies from 0 to 1, that is, the closer this volume is to 1, the better the model predictability. The obtained R^2 volumes indicate the appropriate correlation between the experimental data and this proposed model. The difference between R^2 and Adj-R^2 for the CH_4 conversion percentage, CO/CO_2 molar ratio and H_2 production yield are 0.0089, 0.0107, and 0.0078, respectively, which is <0.2, indicating that the proposed model is acceptable. To enhance this quadratic model validity, the parameters >0.05 P-value are eliminated [9, 40].

The normal probability plot of residuals is another method in evaluating the efficiency of the models [9, 44, 45]. Residual is the difference between the observed and the predicted volumes, which should have a normal or close to the normal distribution, observable through drawing it. The normality of the residuals indicates that the mean of the difference between the residual and the real volume is close to 0 and closer to the residual distribution to 0, the better the designed model. The comparison between the extreme studentized residuals and the CH_4 conversion percentage, S/C ratio, and H_2 production yield together with the real runs are shown in Fig 6 (a-c), indicative of the fact that the distribution data here do not follow a specific pattern, consequently, the independence of the obtained data hypothesis is acceptable.

According to the ANOVA Table, the OC, due to its high F-value has a considerable effect on all the results. The oxidation-reduction cycles' count has the lowest effect on the CH_4 conversion percentage and H_2 production yield, while its significant effect is on the CO/CO_2 molar ratio. Temperature and OC have the highest effect on the CH_4 conversion percentage and H_2 production yield.

By combing the estimates for the variables together with the ANOVA results, the proposed models predicting the CH_4 conversion percentage, CO/CO_2 molar ratio and H_2 production yield through S/W as the response are obtained through Eqs (8-10):

The actual Factors for CH_4 are obtained through Eq.(8):

$$CH_4 = -646.07057 + 2.14071 \times Temperature + 89.66146 \times Catalyst - 0.145833 \times Cycle + 23.32917 \times S/C - 0.09375 \times Temperature \times Catalyst - 0.001606 \times Temperature^2 - 28.82813 \times Catalyst^2 - 4.8125 \times S/C^2 \quad (8)$$

The actual Factors for CO/CO_2 are obtained through Eq. (9):

$$CO/CO_2 = 31.53964 + 0.080006 \times Temperature + 21.19115 \times Catalyst + 0.254427 \times Cycle + 8.58646\ S/C - 0.019063 \times Temperature \times Catalyst - 1.84375 \times Catalyst \times S/C - 0.00005 \times Temperature^2 - 3.86719 \times Catalyst^2 - 0.024922 \times Cycle^2 - 1.09875 \times S/C^2 \quad (9)$$

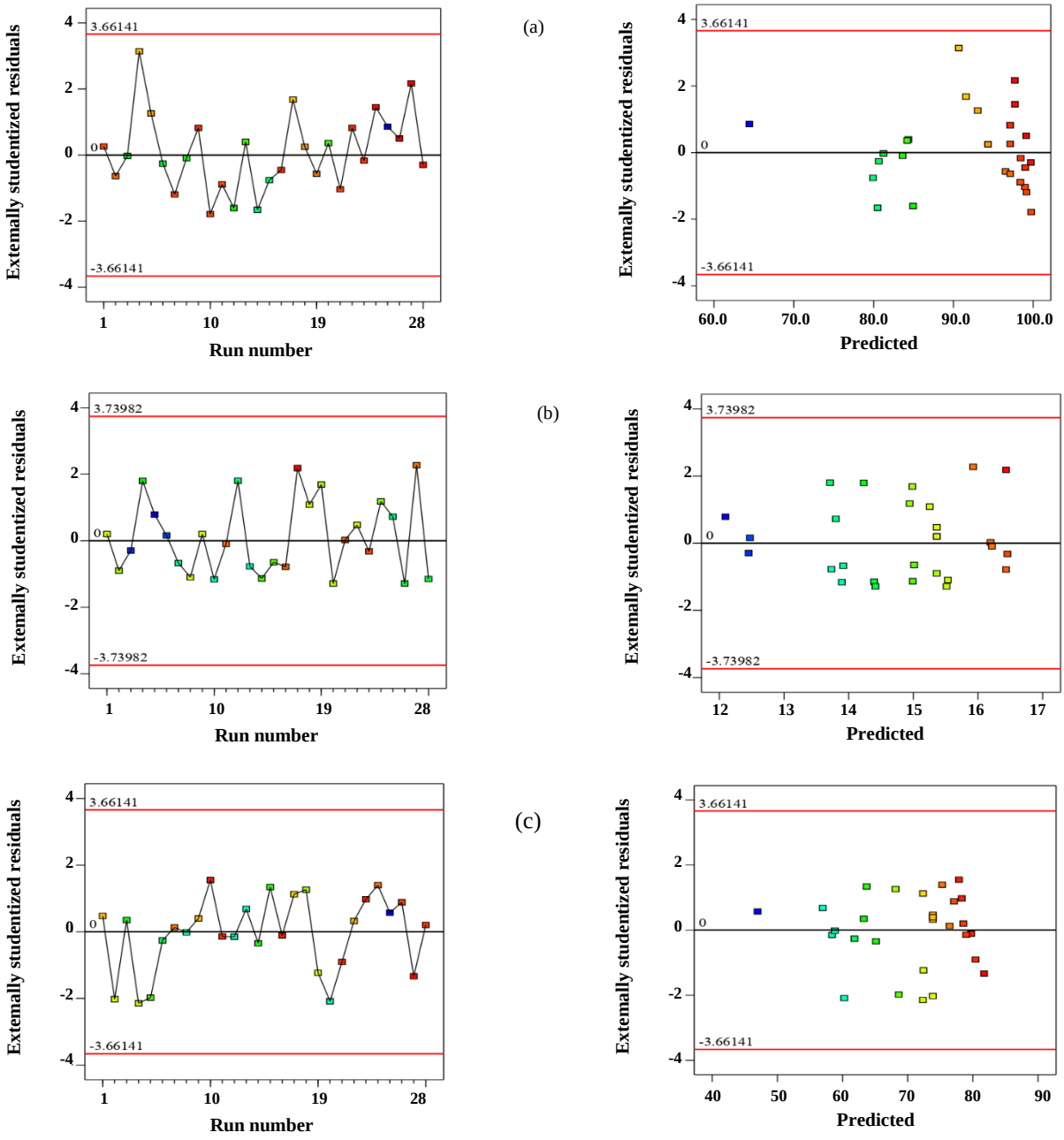

Fig. 6: The residuals vs. predicted and residuals vs. run for a) CH_4 conversion percentage, b) CO/CO_2 molar ratio and c) H_2 production yield

The actual Factors for H_2 are obtained through Eq. (10):

$$H_2 = -358.72031 + 1.24746 \times Temperature - 65.84375 \times Catalyst - 0.358333 \times Cycle + 18.74167 \times S/C + 0.13875 \times Temperature \times Catalyst - 0.000953 \times Temperature^2 - 22.65625 \times Catalyst^2 - 3.375 \times S/C^2 \quad (10)$$

The effect of the variables and their interaction on the CH_4 conversion percentage CO/CO_2 molar ratio, and H_2 production yield

According to the experiments designed through the experiment S/W, first, the OCs are synthesized through different Ni and Mn ratios by adopting the chemical precipitation method and next, assessed subject to different operational conditions in a fixed-bed quartz reactor.

Table 5: ANOVA of the response surface quadratic models.

Source	CH_4 conversion (R_1)		CO/CO_2 (R_2)		H_2 yield (R_3)	
	F-value	p-value	F-value	p-value	F-value	p-value
Model	110.23	< 0.0001 Significant	91.85	< 0.0001 Significant	125.73	< 0.0001 significant
A-Temperature	690.92	< 0.0001	156.37	< 0.0001	886.99	< 0.0001
B-Catalyst	8.39	0.0092	36.15	< 0.0001	12.94	0.0019
C-Cycle	0.8498	0.3682	0.061	0.8092	6.03	0.0239
D-S/C	1.34	0.2609	652.76	< 0.0001	10.23	0.0047
AB	5.85	0.0257	13.42	0.0019	15.07	0.0010
BD	-	-	12.56	0.0025	-	-
A^2	171.82	< 0.0001	8.61	0.0093	71.02	< 0.0001
B^2	14.17	0.0013	13.26	0.0020	10.29	0.0046
C^2	-	-	5.51	0.0313	-	-
D^2	15.42	0.0009	41.81	< 0.0001	8.92	0.0076
Lack of Fit	2.72	0.223	4.06	0.1372	0.8881	0.6319
	not significant		not significant		not significant	
Fit Statistics						
Std. Dev.	1.55		0.2081		1.43	
Mean	91.66		14.80		70.32	
C.V. %	1.69		1.41		2.03	
R^2	0.9789		0.9818		0.9815	
Adjusted R^2	0.9700		0.9711		0.9737	
Predicted R^2	0.9341		0.9327		0.9480	
Adeq Precision	40.1915		33.4421		42.8916	

The reaction of temperature, metal oxide loading volume,S/C ratio, and oxidation-reduction cycles' count parameters on the CH_4 conversion percentage, CO/CO_2 molar ratio, and H_2 production yield is illustrated in Fig. (7-9).

The variables' effect and their interaction on CH_4 conversion percentage

As observed in ANOVA Table, the A, B, AB, A^2, B^2, and D^2 parameters have a significant effect on the CH_4 conversion percentage and the effect of temperature and loading percentage of Ni_xMn_{1-x} have the highest effect on the CH_4 conversion percentage. The effect of increasing the cycle count on this percentage is insignificant, indicating that the mentioned OC has relatively good stability during the consecutive cycles of oxidation-reduction for CH_4 conversion.

The interaction of temperature and Ni_xMn_{1-x} loading percentage parameters on the CH_4 conversion percentage is illustrated in Fig. (7- a), where it is observed that in operational conditions at 600 °C, S/C=2.5, and x=0.5 in the fifth cycle, the CH_4 conversion percentage is 98.3%, and in case of this temperature increases, the CH_4 conversion percentage would continue its ascending trend. Each stable temperature, change in the x (nickel) volume, increase in nickel, first, increase the CH_4 conversion percentage, and next follows a descending trend. An increase in nickel volume, that is, a decrease in Mn volume at high temperature,

leads to a decrease in CH_4 conversion percentage, hence, making parameter AB one of the effective factors on CH_4 conversion percentage. The results indicate that an increase in temperature percentage increase CH_4 conversion and H_2 production, which correspond to the findings in [46, 47].

The increased interactive effects of temperature and S/C ratio parameters on CH_4 conversion percentage, which is more feasible at higher temperatures, is shown in Fig. 7-b. Because at stable temperature an increase in S/C ratio is ascending at the beginning and then it follows a descending trend, an increase in this ratio is not proper at all times, and this volume must be optimized. The temperature interaction with the redox cycle count on the CH_4 conversion percentage is shown in Fig. 7-c, where at stable temperature by increasing redox cycle count, no considerable reduction is observed in CH_4 conversion, that is, the synthesized OC is of good stability.

The effect of variables and their interaction on CO/CO_2 ratio

The interaction of temperature parameters and Ni_xMn_{1-x} loading percentage in the 5th cycle at S/C=2.5 on the CO/CO_2 the molar ratio is illustrated in Fig. (8), where, it is observed that by increasing the reaction temperature, the CO/CO_2 molar ratio increases. The highest and lowest molar ratios are observed at 650°C and 550°C, respectively. The Ni_xMn_{1-x} loading percentage has a considerable effect on CO_2 production. An increase in the loaded Ni volume (for $x > 0.6$), increases the CO_2 production. Low functionality of oxygen in the OC network leads to resistance of OC vs carbon sedimentation [16]. The capability of Mn ferrite in oxygen transfer is low and the oxygen does not release its network easily [18] which leads to a reaction with oxygen scarcity, thus a defective reaction, considered as an advantage in H_2 production. Oxygen-free ferrite and even their reduced products can improve the OC network through CO_2 oxidation, thus a decrease in CO_2 [17]. Consequently, $Ni_xMn_{1-x}Fe_2O_4$ OC is proper for H_2 production, and the presence of Mn in this structure reduces reaction selectivity in relation to CO_2. These results indicate that combination of a few metal oxides together and forming a unit provides the opportunity for their unique positive effect to be applied appropriately, thus one of the advantages in OC.

By decreasing the loaded Ni percentage on the catalyst, its difficulty in lattice oxygen separation from OC, the reaction undergoes more oxygen deficiency and minimize CO_2 production yield, by losing the nickel in the network, and orienting the reaction where selectivity in relation to CO_2 would increase. Consequently, an increase in loaded Ni percentage on the catalyst increase selectivity in relation to CO_2, therefore, adding some Mn may lead the reaction towards oxygen deficiency, and reduce CO_2 production yield. More increase in Mn loading percentage intensifies pore density and blockage, leading to a negative effect on OC activity, something corresponding with the findings in [18, 46].

The variables' effect and their interaction on the H_2 production yield

The effect of temperature, OC loading percentage, S/C ratio, and redox cycle count parameters on the H_2 production yield are shown in Fig. (9). According to the ANOVA table, parameters A, B, C, D, AB, A^2, B^2, and D^2 have a considerable effect on the H_2 production yield, likewise, the temperature, OC loading percentage, S/C ratio parameters, except the increase in cycle count indicate that this OC has relatively good stability.

The S/C ratio is essential in the SMR process. An increase in steam concentration leads to a reduction in CO concentration, thus, an increase in H_2 production yield, while this phenomenon is not always accepted, because it reduces efficiency and increases operational costs, consequently, adjusting the S/C ratio molar is of high essence [48-51]. As observed in Fig. (9-a), in the 3rd cycle at 625°C and increasing the S/C ratio, the H_2 production yield, first, begins an ascending trend and next, a descending, indicating that increasing the S/C ratio in the SMR process is not always a proper measure, and its volume must be optimized.

By increasing the redox count (the time the catalyst is applied) it is expected that the oxygen in the OC network should decrease, thus a reduction in both the H_2 production yield efficiency and CH_4 conversion percentage. As observed in Fig. (9-b), when reaction temperature, loading percentage, and S/C ratio are constant, an increase in the redox cycle is not significant in the H_2 production yield. This is due to the almost or complete oxygen-free ferrite capable of compensating its oxygen network through CO_2 oxidation and cause a reduction in CO_2 production [13, 17, 43].

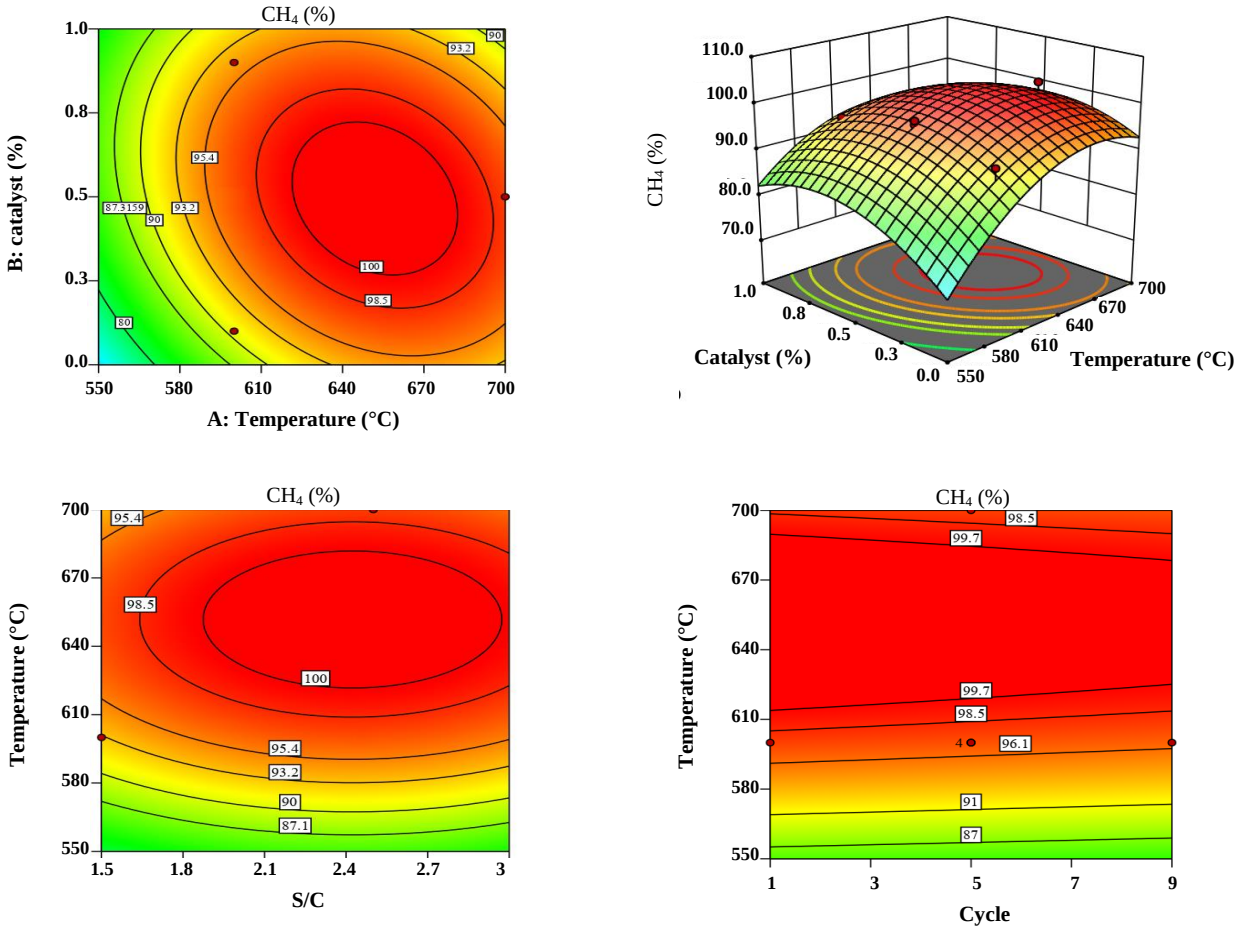

Fig. 7: The effect of the variables and their interaction on the responses CH_4 conversion percentage.

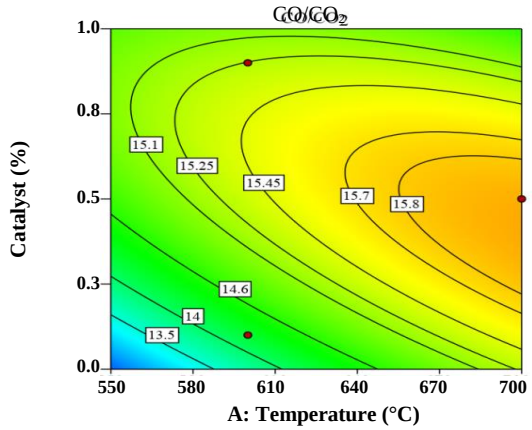

Fig. 8: The effect of the variables and their interaction on the responses CO/CO_2.

The temperature and $Ni_xMn_{1-x}Fe_2O_4$ loading percentage during 9 cycles and S/C=2.5 are shown in Fig. (9-c). The results indicate that by increasing, reaction temperature from 550°C to 650°C at X=0.4, the H_2 production yield temperature increase from 61.37 to 78.43%. Likewise, the loading percentage of X concentration in $Ni_xMn_{1-x}Fe_2O_4$ OC has a significant effect on H_2 production yield, and the more the Ni volume in loading the less H_2 production yield [13, 17].

In the reforming process, pure nickel leads to the selectivity of the process towards complete oxidation CO_2 and H_2O production. The co-existence of Nickel and Iron and their spinal structure indicate that the synthesized $NiFe_2O_4$ is of high ability in redox and can be applied as an OC for H_2 production [13, 17, 18, 52, 53]. If this Iron-based OC spinal structure collapses and forms the α-Fe_2O_3 phase the CO and H_2 are converted into H_2O and CO_2 [8]. It is accepted by increasing the cycle count this phenomenon would persist and lead to coke formation on the catalyst surface, which is no proper CH_4 cracking and a reduction in H_2 production yield. As observed in Figs. 7 and 9, the CH_4 conversion means and H_2 production yield mean percentage at 9 consecutive redox cycles remain

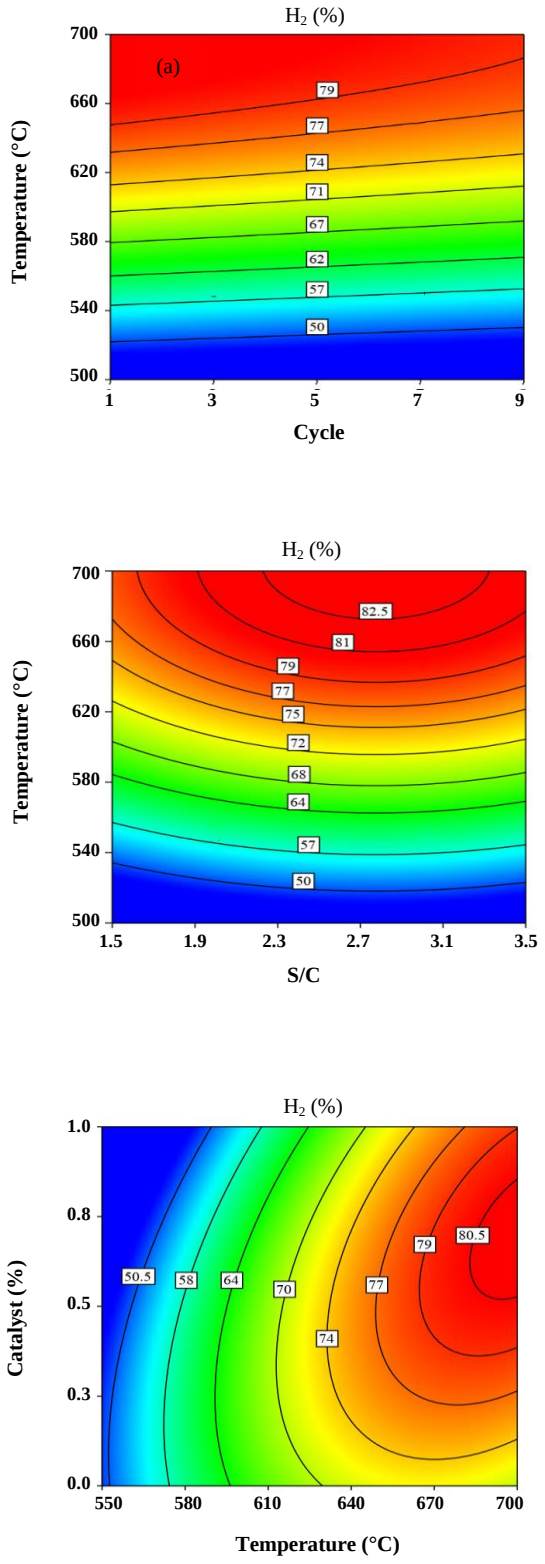

Fig. 9: The effect of the variables and their interaction on the responses H_2 production yield

almost stable, that is no spinal construct collapse or if any, very slight. These results do not correspond to that of [8-10, 13, 14, 18]. After different consecutive redox cycles, no significant structural change occurred in the OC.

The advantages of the OCs are: high consistency, high CH_4 conversion percentage mean, high H_2 production yield, and low carbon production on the catalyst surface at 9 consecutive cycles.

Optimization

The model analysis results are assessed and the optimum state of the CH_4 conversion volumes, CO/CO_2 molar ratio and H_2 production yield are obtained through the experiment design S/W. This optimization is run within -1 to +1 levels for all the basic parameters, where the objective is to increase the H_2 production yield and CH_4 conversion percentage.

Adopting the appropriateness method in optimizing the parameters can contribute to finding the best possible solution. The appropriate conditions of each independent variable, capable of obtaining the maximum H_2 production and CH_4 conversion percentage and minimum CO/CO_2 molar ratio are determined through the appropriateness functionality [54]. To achieve this objective, the variables consisting of reaction temperature (550-700°C), OC loading percentage (0.1-0.9), S/C (1.5-3), and redox cycles' count (1-9) are determined based on their level of importance as the appropriate conditions, Table (6).

After determining the restrictions to maximize the H_2 production yield and the CH_4 conversion percentage and to minimize the CO/CO_2 molar ratio within the independent variables' range, the RSM S/W is applied, were subject to the imposed conditions, 14 experiments are proposed within 0.98-0.96 appropriateness range, Table 7. After optimization, the synthesized samples' catalyst functionalities are assessed based on the experiments designed in a quartz reactor. The effect of the variables and the interaction thereof on the CH_4 conversion percentage, CO/CO_2 molar ratio and H_2 production yield in this proposed optimized model is compared with that of the laboratory result, Table 8.

This proposed optimization model consists of: independent factors of 650°C, Ni_XMn_{1-X} (X=0.62) loading percentage, S/C=2.48 ratio, and 9 cycles with reactive responses consisting of CH_4 conversion percentage,

Table 6: The restrictions imposed in determining the appropriateness functionality.

Name	Goal	Lower Limit	Upper Limit	Lower Weight	Upper Weight	Importance
A:Temperature	is in range	550	700	1	1	1
B:Catalyst	is in range	0.1	0.9	1	1	1
C:Cycle	Maximize	1	9	1	1	1
D:S/C	is in range	1.5	3	1	1	1
CH_4	Maximize	65.3	99.8	1	1	1
CO/CO_2	is in range	12.2	16.7	1	1	1
H_2	Maximize	47.5	80.5	1	1	1

Table 7: The optimized conditions obtained for H_2 production yield, CH_4 conversion percentage, and CO/CO_2 molar ratio based on their appropriateness.

Number	Temperature	Catalyst	Cycle	S/C	CH_4 conversion	CO/CO_2	H_2 yield	Desirability
1	649.9	0.55	9	2.87	99.8	16.02	78.9	0.98
2	650	0.62	9	2.48	100	15.33	78.6	0.98
3	649	0.62	9	2.78	99.8	15.83	78.7	0.98
4	650	0.66	9	2.58	99.94	15.49	78.5	0.98
5	649	0.63	9	2.81	99.5	15.85	78.7	0.98
6	650	0.67	9	2.50	99.9	15.34	78.3	0.98
7	642	0.51	9	2.68	100	15.71	78.3	0.97
8	649.9	0.54	9	2.31	100	14.96	78.3	0.97
9	647.7	0.68	9	2.56	99.7	15.43	78.1	0.97
10	639.6	0.53	9	2.74	100	15.78	78	0.97
11	650	0.69	9	2.39	99.7	15.10	77.9	0.97
12	641.5	0.59	9	2.56	100	15.47	77.9	0.97
13	649.9	0.62	9	2.07	99.8	14.33	77.1	0.96
14	647.2	0.59	8.6	2.44	100	15.31	78.4	0.96

Table 8: The proposed optimized model results compared to that of the laboratory.

Model type	Temperature	Catalyst	Cycle	S/C	CH_4	CO/CO_2	H_2	CO
Suggested	650	0.62	9	2.48	100	15.33	78.6	-
Experimental	650	0.6	9	2.5	99.6	15.7	77. 6	18.2

CO/CO_2 molar ratio, and H_2 production yield of 100%, 15.33, and 78.6%, respectively with 98% confidence factor. To evaluate this model the proposed conditions are close to that of laboratory implementation. Here, the adjustments are made in a quartz reactor (three iterations) at 650°C, loading percentage $Ni_XMn_{1-X}Fe_2O_4$ (x=0.6), CO/CO_2 molar ratio in 9 cycles, and the obtained percentages consist of 99.6, 15.7, and 77.6, respectively which are acceptable.

To run the structural analysis and determine the chemical composition of the optimized sample before and after the reactor test, the FE-SEM together with EDX

Table 9: Physical characteristics of the fresh and used OCs.

Sample	D_{XRD} (nm)	D_{SEM} (nm)	S_{BET} (m^2/g)	Vp (cm^3/g)	dp (nm)
$Ni_{0.6}Mn_{0.4}Fe_2O_4$ (fresh)	36	41	6.54	0.017	12.86
$Ni_{0.6}Mn_{0.4}Fe_2O_4$ (used)	78	84	1.69	0.0093	26.76

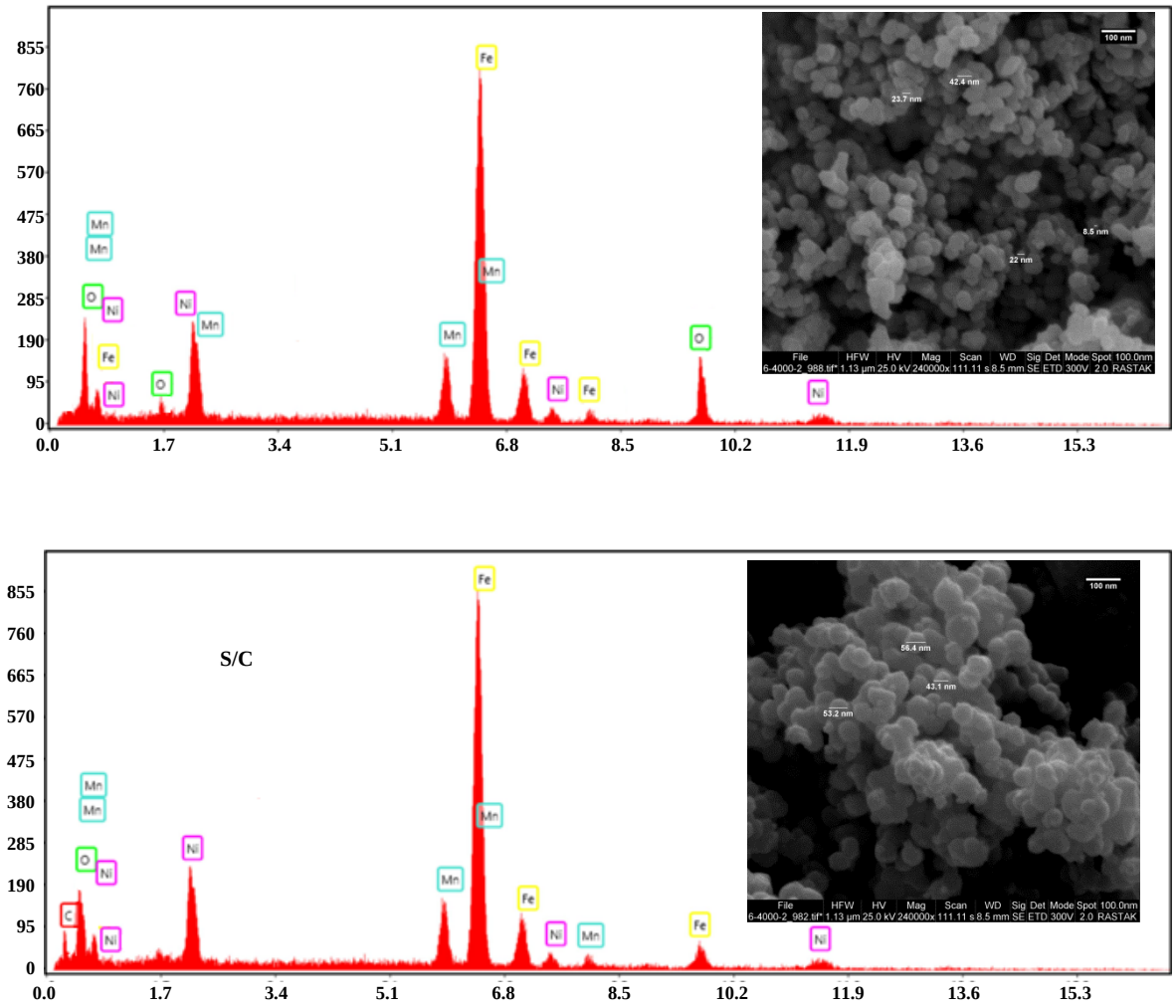

Fig. 10: FE-SEM and EDX analysis and the available elements' level therein: a) the $Ni_{0.6}Mn_{0.4}Fe_2O_4$ OC, b) the $Ni_{0.6}Mn_{0.4}Fe_2O_4$ OC after reactor test at 650 ℃ and S/C=2.5 in 9 redox cycles

the analysis is run. Each one of the spectra peaks yields from EDX is attributed to a specific atom. The higher the element peak, the more the concentration therein. The FE-SEM analysis and the spectrum obtained from the synthesized sample through EDX together with the elemental compositions of the elements in the sample analyzed through weight percentage are illustrated in Fig. 10-a, where, it is observed that the OC particles' size is within 20 to 80 nm range with a spherical shape and no impurity. The FE-SEM and EDX analyses of the applied sample are illustrated in Fig. 10-b, where it is observed that the particle size is bigger than the case where the sample is not applied in the reactor and there exist impurities on the surface of the OC. The XRD analysis of the OC applied in the reactor after 9 redox cycles are illustrated in Fig. 3-b. The spectrum obtained from this analysis indicates the existence of impurities on the surface of the catalyst is due to the carbon production therein.

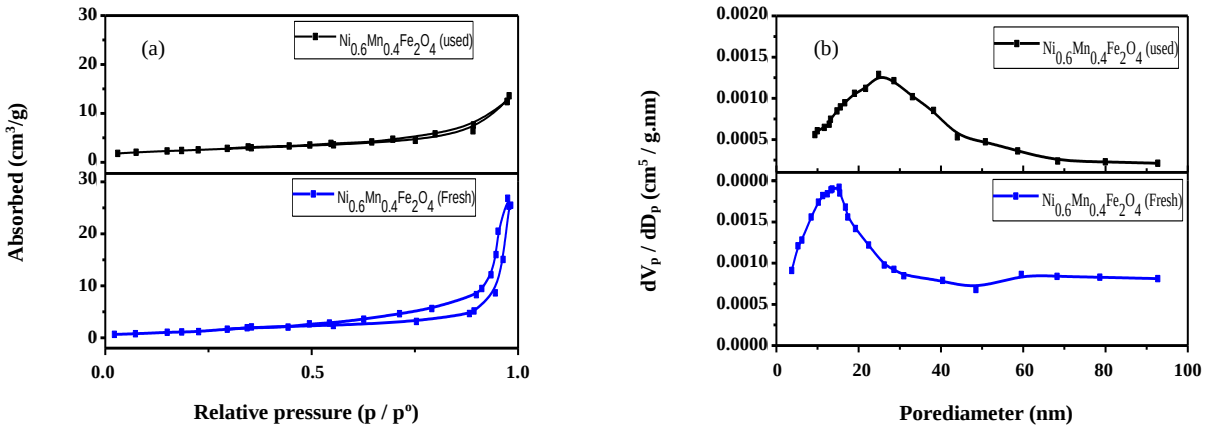

Fig. 11: a) N_2 adsorption-desorption isotherms distribution of fresh and used OCs and b) pore size distribution of fresh and used OCs

The FE-SEM, EDX, and XRD analyses' results approve the existence of carbon on the catalyst surface. Unlike observations in [8-16], in the applied XRD sample spectrum, during 9 redox cycles, no trace of the unwanted Fe_2O_3 is observed which would lead to the conversion of CO, H_2 to CO_2, and H_2O.

The N_2 adsorption-desorption isotherms of optimized $Ni_{0.6}Mn_{0.4}Fe_2O_4$ OC prior, (synthesized sample) and after, (applied sample) reactor test are shown in Fig. 11 a and b, indicating that the isotherm curve and pore size are of H1.

The physical properties of the same are tabulated in Table 9. The results obtained from BET and BJH tests on OCs indicate that due to pore blockage, the specific surface of OC is reduced, that is, the specific surface of OC $Ni_{0.6}Mn_{0.4}Fe_2O_4$ after 9 redox cycles is reduced from 6.54 to 1.69, a 74.16% reduction with an increase in pore diameter from 12.86 to 26.76, about 2.08 fold in average. Consequently, the results of BJH, BET, XRD, EDX, and FE-SEM verify the formation of coke on the catalyst surface.

Coke formation

The formation of carbon on the surface of the catalyst in the SMR process is one of the most important reasons for the inactivation of catalysts. Three types of carbonaceous species are formed on the Ni-based catalysts [55, 56]. The monoatomic carbon species (C_α) are oxidized at a temperature lower than 400°C and act as a reaction intermediate and are mainly responsible for syngas formation. The formation of C_α species does not affect the inactivation of the catalyst [55-58].

C_β species are oxidized at 500–600°C and are usually transformed from amorphous carbon, C_α, and have a high possibility to change into encapsulating carbon (C_γ). Graphite carbon species and C_γ are formed at temperatures higher than 650°C and are the most stable form of carbonaceous species [56, 58]. They can only be oxidized at high temperatures and are the main causes of catalyst deactivation. The formation and accumulation of C_β and C_γ species can deactivation the catalyst by covering the active surface of nickel metal. An example of the TGA analyses of the used catalyst obtained with a reaction temperature at 650 °C and S/C=2.5 in 24 cycles is shown in Fig. 12.

The initial weight loss within the 30- 300°C range is related to some easily oxidized carbon species removal like amorphous. The weight increases within the 300-400°C range. This is because Ni particles in the applied catalysts are oxidized into NiO more rapidly than fresh catalysts during this period**.** Weight loss of at higher than 500°C is due to the oxidation of carbon graphics into CO_2**.** The mass percentage of carbonaceous species over the used OC, measured from TGA analyses is shown in Table 12. The total volume percentage of carbon formed on the surface of the catalyst used at the reaction temperature at 650 °C and S/C=2.5 in 24 cycles reaches 7.16%. It can be deduced that $Ni_{0.6}Mn_{0.4}Fe_2O_4$ OC prevents the formation of the inactive C_β and $C\gamma$ species carbon species and maintains catalytic activity because the lattice oxygen in $Ni_{0.6}Mn_{0.4}Fe_2O_4$ enhances the C_β and $C\gamma$ species oxidation.

Table 12: The TGA analyses of used $Ni_{0.6}Mn_{0.4}Fe_2O_4$ OC after reactor test at 650 ℃ and S/C=2.5 in 24 redox cycles.

Used catalysts	C_β (%)	C_α (%)	C_γ (%)	Total coke formation (%)
$Ni_{0.6}Mn_{0.4}Fe_2O_4$	2.53	4.63	0	7. 16

Table 13: Element compositions of Ni0.6Mn0.4Fe2O4 OC fresh and used after reactor test at 650 ℃ and S/C=2.5 in 9 redox cycles.

OC	Fe	Mn	O	Ni	C
$Ni_{0.6}Mn_{0.4}Fe_2O_4$ fresh	48.76	11.43	20.09	19.72	0
$Ni_{0.6}Mn_{0.4}Fe_2O_4$ used	47.60	11.08	15.81	18.24	7.27

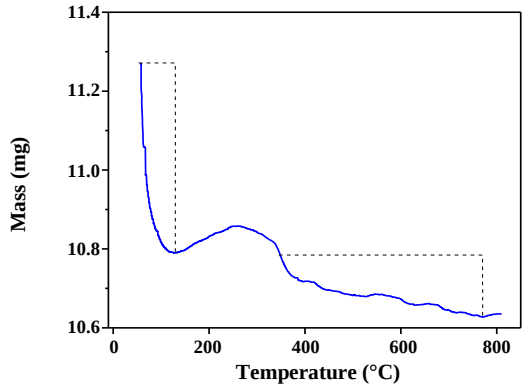

Fig. 12: TGA profile of the used catalyst obtained with a reaction temperature of 650 °C and S/C=2.5 in 24 cycles.

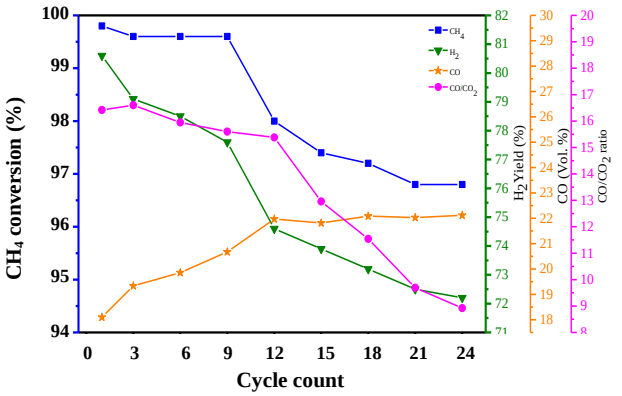

Fig. 13: $Ni_{0.6}Mn_{0.4}Fe_2O_4$ OC in 24 redox cycles at 650°C and S/C=2.5.

Furthermore, the elemental compositions of fresh and used OCs can be obtained from EDX images, and its exact volume is tabulated in Table 13, where slight coke formation is evident on the surface of the used OC. Although this volume is not the same as the TGA results, it exposes the same order.

Oxygen carier stability

To evaluate the stability and functionality of the $Ni_{0.6}Mn_{0.4}Fe_2O_4$ OC in 24 redox cycles, at 650°C with S/C=2.5 is assessed. The CH_4 conversion, H_2 production yield, CO/CO_2 ratio, and the produced CO are shown in Fig. 13, where, the CH_4 conversion percentage in 24 redox cycle is reduced by 3%, likewise the H_2 production yield from 80.2% to 73%, while the volume of CO_2 production increased from 18.1 to 22.2. It is deduced that after 24 consecutive redox cycles of oxidation/reduction no structural change occurs in this synthesized OC and the self-supported $Ni_{0.6}Mn_{0.4}Fe_2O_4$ can be reduced again (Fe -M and wustite) Fe_xO alloys and prevent α-Fe_2O_3 CO formation. High stability, high CH_4 conversion percentage, high H_2 production yield, and relatively low carbon formation on the catalyst surface in 24 consecutive cycles is the advantage of this OC in relation to that of Mn, Cu, Co, and Ni spinal ferrite OC [17, 18, 59], Perovskite OC [10, 60, 61], and Iron-based OC [9, 10, 43, 60, 61].

CONCLUSIONS

In this study, the $Ni_xMn_{1-x}Fe_2O_4$ OCs are synthesized by adopting the chemical sedimentation method which is implemented in synthesized gas production in CL-SMR for the first time. Due to different conditions in this process, the RSM model is applied based on the CCD model to evaluate the effect of the independent parameters on responses and better production as to the response volume.

The results indicate that reaction temperature and metal oxides loading rate are the most important features affecting both the CH_4 conversion percentage and H_2 production yield increase and that the oxidation cycle count has low effect on the last two parameters' effect.

To evaluate and validate this optimization model through

designing laboratory tests by adjusting the conditions therein, the CH_4 conversion percentage, CO/CO_2 ratio, and H_2 production yield of 99.6, 15.7, and 77.6 are obtained, respectively. By integrating different metal oxides, different spinal structures are formed which would be able to share their unique proportions and facilitate reaction occurrence and provide more appropriate selectivity therein. At the presence of Ni in OC formation, a considerable volume of oxygen is in access, thus more tendencies in producing CO_2. Here, by adding Mn element in OC formation, due to lack of oxygen in OC-construction, the stability of reaction in relation to CO_2 production reaction is enhanced. Evaluation of the optimized OC functionality and stability in the 24 redox cycles indicates that the self-supported $Ni_{0.6}Mn_{0.4}Fe_2O_4$ is of high stability and high CH_4 conversion percentage, and H_2 production yield with proportionally low carbon production.

In this article, as expected, within the rational response volume range, it is found that applying integrating metals like Mn, Ni, Co, and Cu with M-Fe_2O_4 in the CL-SMR process is promising. Though the optimized OC is of relatively good performance, due to coke formation on the OC surface is necessary to add a series of parameters that will be studied and assessed through this research group.

Received : Feb. 2, 2020 ; Accepted : June 8,2020

REFERENCES

[1] Udomchoke T., Wongsakulphasatch S., Kiatkittipong W., Arpornwichanop A., Khaodee W., Powell J., Performance Evaluation of Sorption Enhanced Chemical-Looping Reforming for Hydrogen Production from Biomass with Modification of Catalyst and Sorbent Regeneration, *Chem. Eng. J.*, **303**: 338-347 (2016).

[2] Mehrypooya M., Moftakhari Sharifzadeh M., Design of an Integrated Process for Simultaneous Chemical Looping Hydrogen Production and Electricity Generation with CO_2 Capture, *International Journal of Hydrogen Energy*, **42(12)**. 8486-8496 (2017).

[3] Rydén M., Ramos P., H_2 Production with CO_2 Capture by Sorption Enhanced Chemical-Looping Reforming Using NiO as Oxygen Carrier and CaO as CO_2 Sorbent, *Fuel Process. Technol.*, **96**: 27–36 (2012).

[4] Nadgouda S.G., Kathe M.V., Fan L.S., Cold Gas Efficiency Enhancement in a Chemical Looping Combustion System Using Staged H_2 Separation Approach, *International Journal of Hydrogen Energy*, **42(8)**: 4751-4763 (2017).

[5] Zhang Y., Chao Z., Jakobsen H.A., Modelling and Simulation of Hydrodynamics in Double Loop Circulating Fluidized Bed Reactor for Chemical Looping Combustion Process, *Powder Technology*, **310**: 35-45 (2017).

[6] Luo M., Yi Y., Wang S., Wang Z., Du M., Pan J., Wang Q., Article Review of Hydrogen Production Using Chemical-Looping Technology, *Renewable and Sustainable Energy Reviews*, **81**: 3186-3214 (2018).

[7] Protasova L., Snijkers F., Recent Developments in Oxygen Carrier Materials for Hydrogen Production *via* Chemical Looping Processes, *Fuel*, **181**: 75-93 (2016).

[8] Zhongliang Y., Yang Y., Yang S., Zhang Q., Zhao J., Fang Y., Guan G., Iron-based Oxygen Carriers in Chemical Looping Conversions: A Review, *Carbon Resour. Convers.*, (2018).

[9] Forutan H.R., Karimi E., Hafizi A., Rahimpour M.R., Keshavarz P., Expert Representation Chemical Looping Reforming: A Comparative Study of Fe, Mn, Co and Cu as Oxygen Carriers Supported on Al_2O_3, *J. Ind. Eng. Chem.*, **21**: 900–911 (2015).

[10] Lim H.S., Kang D., Lee J.W., Phase Transition of Fe_2O_3-NiO to $NiFe_2O_4$ in Perovskite Catalytic Particles for Enhanced Methane Chemical Looping Reforming-Decomposition with CO_2 Conversion, *Appl. Catal. B Environ.*, **202**: 175-183 (2017).

[11] Miller D.D., Siriwardane R., Poston J., Fluidized-Bed and Fixed-Bed Reactor Testing of Methane Chemical Looping Combustion with MgO-Promoted Hematite, *Applied Energy*, **146**: 111-121 (2015).

[12] Johansson M., Screening of Oxygen-Carrier Particles Based on Iron, Manganese, Copper and Nickel Oxides for Use in Chemical-Looping Technologies. Chalmers University of Technology Göteborg, Sweden, (2007).

[13] Huang Z., He F., Chen D., Zhao K., Wei G., Zheng A., Li H., Investigation on Reactivity of Iron-Nickel Oxides in Chemical Looping Dry Reforming, *Energy*, **116**: 53-63 (2016).

[14] Zhu M., Song Y., Chen S., Li M., Zhang L., Xiang W., Chemical Looping Dry Reforming of Methane with Hydrogen Generation on Fe_2O_3/Al_2O_3 Oxygen Carrier, *Chem. Eng. J.*, **368**: 812–823 (2019).

[15] Lin C., Qin W., Dong C., Reduction Effect of α-Fe_2O_3 on Carbon Deposition and CO Oxidation During Chemical-Looping Combustion, *Chem. Eng. J.*, **301**: 257–265 (2016).

[16] Huang J., Liu W., Hu W., Metcalfe I., Yang Y., Liu B., Phase Interactions in Ni-Cu-Al_2O_3 Mixed Oxide Oxygen Carriers for Chemical Looping Applications, *Appl. Energy*, **236**: 635-647 (2019).

[17] Huang Z., Jiang H., He F., Chen D., Wei G., Zhao K., Li H., Evaluation of Multi-Cycle Performance of Chemical Looping Dry Reforming Using CO_2 as an Oxidant with Fe-Ni Bimetallic Oxides, *J. Energy Chem.*, **25(1)**: 62–70 (2016).

[18] Evdou A., Zaspalis V., Nalbandian L., Ferrites as Redox Catalysts for Chemical Looping Processes, *Fuel*, **165**: 367–378 (2016).

[19] Aston V.J., Evanko B.W., Weimer A.W., Investigation of Novel Mixed Metal Ferrites for Pure H_2 and CO_2 Production Using Chemical Looping, *Int. J. Hydrogen Energy*, **38(22)**: 9085–9096 (2013).

[20] Ismail M., Liu W., Dunstan M.T., Scott S.A., Development and Performance of Iron-Based Oxygen Carriers Containing Calcium Ferrites for Chemical Looping Combustion and Production of Hydrogen, *International Journal of Hydrogen Energy*, **41(7)**: 4073-4084 (2016).

[21] Ma S., Chen S., Soomro A., Xiang W., Effects of Supports on Hydrogen Production and Carbon Deposition of Fe-Based Oxygen Carriers in Chemical Looping Hydrogen Generation, *International Journal of Hydrogen Energy*, **42(16)**: 11006–11016 (2017).

[22] De Vos Y., Jacobs M., Van Der Voort P., Van Driessche I., Snijkers F., Verberckmoes A., Sustainable Iron-Based Oxygen Carriers for Chemical Looping for Hydrogen Generation, *Int. J. Hydrogen Energy*, **44(3)**: 1374-1391 (2019).

[23] Nadgouda S.G., Guo M., Tong A., Fan L.-S., High Purity Syngas and Hydrogen Coproduction Using Copper-Iron Oxygen Carriers in Chemical Looping Reforming Process, *Appl. Energy*, **235**: 1415–1426 (2019).

[24] Chen J., Zhao K., Zhao Z., He F., Huang Z., Wei G., Identifying the Roles of MFe_2O_4 (M= Cu, Ba, Ni, and Co) in the Chemical Looping Reforming of Char, Pyrolysis Gas and Tar Resulting from Biomass Pyrolysis, *Int. J. Hydrogen Energy*, **44(10)**: 4674-4687 (2019).

[25] Liu F., Liu J., Yang Y., Wang Z., Zheng C., Reaction Mechanism of Spinel $CuFe_2O_4$ with CO During Chemical-Looping Combustion: an Experimental and Theoretical Study," *Proc. Combust. Inst.*, **37(4)**: 4399-4408 (2019).

[26] Pérez-Vega R., Abad A., Izquierdo M.T., Gayán P., de Diego L.F., Adánez J., Evaluation of Mn-Fe mixed Oxide Doped with TiO_2 for the Combustion with CO_2 Capture by Chemical Looping Assisted by Oxygen Uncoupling, *Appl. Energy*, **237**: 822–835 (2019).

[27] Källén M., Rydén M., Lyngfelt A., Mattisson T., Chemical-Looping Combustion Using Combined Iron/Manganese/Silicon Oxygen Carriers, *Appl. Energy*, **157**: 330-337 (2015).

[28] Fernández Garcia J. R., Martinez I., Abanades Garcia J.C., Romano M.C., "Conceptual Design of a Ca-Cu Chemical Looping Process for Hydrogen Production in Integrated Steelworks, *Int. J. Hydrogen Energy*, **42(16)**: 11023-11037 (2017).

[29] Ortiz M., Gayán P., Luis F., García-Labiano F., Abad A., Pans M.A., Adánez J., Hydrogen Production With CO_2 Capture by Coupling Steam Reforming of Methane and Chemical-Looping Combustion: Use of an Iron-Based Waste Product as Oxygen Carrier Burning a PSA Tail Gas, *Journal of Power Sources*, **196(9)**: 4370-4381 (2011).

[30] Hallberg P., Hanning M., Rydén M., Mattisson T., Lyngfelt A., Investigation of a Calcium Manganite as Oxygen Carrier During 99 h of Operation of Chemical-Looping Combustion in a 10 kWth Reactor Unit, *International Journal of Greenhouse Gas Control*, **53**: 222–229 (2016).

[31] Kuo P.-C., Chen J.-R., Wu W., Chang J.-S., Hydrogen Production from Biomass Using Iron-Based Chemical Looping Technology: Validation, Optimization, and Efficiency, *Chem. Eng. J.*, **337**: 405-415 (2018).

[32] Patcharavorachot Y., Chatrattanawet N., Arpornwichanop A., Assabumrungrat S., Optimization of Hydrogen Production from Three Reforming Approaches of Glycerol Via Using Supercritical Water with in Situ CO_2 Separation, *Int. J. Hydrogen Energy*, **44(4)**: 2128–2140 (2019).

[33] Fard A.A., Arvaneh R., Alavi S. M., Bazyari A., Valaei A., Propane Steam Reforming over Promoted Ni-Ce/$MgAl_2O_4$ Catalysts: Effects of Ce Promoter on the Catalyst Performance Using Developed CCD Model, *Int. J. Hydrogen Energy*, **44(39)**: 21607–21622 (2019).

[34] Maaz K., Duan J. L., Karim S., Chen Y. H., Zhai P. F., Xu L.J., Liu J., Fabrication and Size-Dependent Magnetic Studies of NixMn1- xFe_2O_4 (x= 0.2) Cubic Nanoplates, *J. Alloys Compd.*, **684**: 656–662 (2016).

[35] Sun Y., Diao Y., Wang H., Chen G., Zhang M., Guo M., Synthesis, Structure and Magnetic Properties of Spinel Ferrite (Ni, Cu, Co) Fe_2O_4 from Low Nickel Matte, *Ceram. Int.*, **43(18)**: 16474–16481 (2017).

[36] Patterson A.L., The Scherrer Formula for X-Ray Particle Size Determination, *Phys. Rev.*, **56(10)**:978- (1939).

[37] Taghavi Fardood S., Ebadzadeh B., Ramazani A., Green Synthesis and Characterization of Ni-Cu-Mg Ferrite Nanoparticles in the Presence of Tragacanth Gum and Study of Their Catalytic Activity in the Synthesis of Hexanitrohexaazaisowurtzitane, *Iran. J. Chem. Chem. Eng*. **38(6)**: 21-29 (2019).

[38] Stoia M., Muntean E., P\uacurariu C., Mihali C., Thermal Behavior of $MnFe_2O_4$ and $MnFe_2O_4$/C Nanocomposite Synthesized by a Solvothermal Method, *Thermochim. Acta*, **652**: 1–8 (2017).

[39] Hafizi A., Rahimpour M. R., Hassanajili S., Calcium Promoted Fe/Al_2O_3 Oxygen Carrier for Hydrogen Production *via* Cyclic Chemical Looping Steam Methane Reforming Process, *Int. J. Hydrogen Energy*, **40(46)**: 16159-16168 (2015).

[40] Hafizi A., Jafari M., Rahimpour M.R., Hassanajili S., Experimental Investigation of Sorption Enhanced Chemical Looping Reforming for High Purity Hydrogen Production Using CeO_2-CaO CO_2 Sorbent and 15Fe-5Ca/Al_2O_3 Oxygen Carrier, *J. Taiwan Inst. Chem. Eng.*, **65**: 185–196 (2016).

[41] Forutan H.R., Karimi E., Hafizi A., Rahimpour M.R., Keshavarz P., Expert Representation Chemical Looping Reforming: A Comparative Study of Fe, Mn, Co and Cu as Oxygen Carriers Supported on Al_2O_3, *J. Ind. Eng. Chem.*, **21**: 900–911 (2015).

[42] Hossain M.A., Ayodele B.V., Cheng C.K., Khan M.R., Optimization of Renewable Hydrogen-Rich Syngas Production from Catalytic Reforming of Greenhouse Gases (CH_4 and CO_2) over Calcium Iron Oxide Supported Nickel Catalyst, *J. Energy Inst.*, **92(1)**: 177–194 (2019).

[43] Hafizi A., Rahimpour M. R., Hassanajili S., Hydrogen Production by Chemical Looping Steam Reforming of Methane over Mg Promoted Iron Oxygen Carrier: Optimization Using Design of Experiments, *J. Taiwan Inst. Chem. Eng.*, **62**: 140–149 (2016).

[44] Hafizi A., Ahmadpour A., Heravi M.M., Bamoharram F.F., Khosroshahi M., Alkylation of Benzene with 1-Decene Using Silica Supported Preyssler Heteropoly Acid: Statistical Design with Response Surface Methodology, *Chinese J. Catal.*, **33(2–3)**: 494–501 (2012).

[45] Hafizi A., Ahmadpour A., Koolivand-Salooki M., Heravi M. M., Bamoharram F. F., Comparison of RSM and ANN for the Investigation of Linear Alkylbenzene Synthesis over H_{14} [$NaP_5W_{30}O_{110}$]/SiO_2 Catalyst, *J. Ind. Eng. Chem.*, **19(6)**: 1981–1989 (2013).

[46] Alirezaei I., Hafizi A., Rahimpour M.R., Syngas Production In Chemical Looping Reforming Process over ZrO_2 Promoted Mn-Based Catalyst, *J. CO_2 Util.*, **23**: 105–116 (2018).

[47] Frick V., Rydén M., Leion H., Investigation of Cu-Fe and Mn-Ni Oxides as Oxygen Carriers for Chemical-Looping Combustion, *Fuel Process. Technol.*, **150**: 30-40 (2016).

[48] He F., Wei Y., Li H., Wang H., Synthesis Gas Generation by Chemical-Looping Reforming Using Ce-Based Oxygen Carriers Modified with Fe, Cu, and Mn Oxides, *Energy & Fuels*, **23(4)**: 20952102 (2009).

[49] Meshksar M., Daneshmand-Jahromi S., Rahimpour M.R., Synthesis and Characterization of Cerium Promoted Ni/SBA-16 Oxygen Carrier in Cyclic Chemical Looping Steam Methane Reforming, *J. Taiwan Inst. Chem. Eng.*, **76**: 73–82 (2017).

[50] Dou B., Song Y., Wang C., Chen H., Yang M., Xu Y., Hydrogen Production by Enhanced-Sorption Chemical Looping Steam Reforming of Glycerol in Moving-Bed Reactors, *Appl. Energy*, **130**: 342–349 (2014).

[51] Akbari-Emadabadi S., Rahimpour M. R., Hafizi A., Keshavarz P. Production of Hydrogen-Rich Syngas Using Zr Modified Ca-Co Bifunctional Catalyst-Sorbent in Chemical Looping Steam Methane Reforming, *Appl. Energy*, **206**: 51-62 (2017).

[52] Pena J.A., Lorente E., Romero E., Herguido J., Kinetic Study of the Redox Process for Storing Hydrogen: Reduction Stage, *Catal. today*, **116(3)**: 439-444 (2006).

[53] Ma S., Chen S., Soomro A., Xiang W., Effects of Supports on Hydrogen Production and Carbon Deposition of Fe-Based Oxygen Carriers in Chemical Looping Hydrogen Generation, *Int. J. Hydrogen Energy*, **42(16)**: 11006-11016 (2017).

[54] Ayodele B.V., Ghazali A.A., Yassin M.Y.M., Abdullah S., Optimization of Hydrogen Production by Photocatalytic Steam Methane Reforming over Lanthanum Modified Titanium (IV) Oxide Using Response Surface Methodology, *Int. J. Hydrogen Energy*, **44(37)**: 20700-20710 (2019).

[55] Zhang Y., Wang W., Wang Z., Zhou X., Wang Z., Liu C.-J., Steam Reforming of Methane over Ni/SiO_2 Catalyst with Enhanced Coke Resistance at Low Steam to Methane Ratio, *Catal. Today*, **256**: 130-136 (2015).

[56] Cheng D., Zhu X., Ben Y., He F., Cui L., Liu C., Carbon Dioxide Reforming of Methane over Ni/Al_2O_3 Treated with Glow Discharge Plasma, *Catal. Today*, **115(1-4)**: 205-210 (2006).

[57] Zhai X., Ding S., Liu Z., Jin Y., Cheng Y., Catalytic Performance of Ni Catalysts for Steam Reforming of Methane at High Space Velocity, *Int. J. Hydrogen Energy*, **36(1)**: 482-489 (2011).

[58] Urasaki K., Sekine Y., Kawabe S., Kikuchi E., Matsukata M., Catalytic Activities and Coking Resistance of Ni/Perovskites in Steam Reforming of Methane, *Appl. Catal. A Gen.*, **286(1)**: 23-29 (2005).

[59] Siriwardane R., Tian H., Miller D., Richards G., Fluidized Bed Testing of Commercially Prepared MgO-Promoted Hematite and CuO–Fe_2O_3 Mixed Metal Oxide Oxygen Carriers for Methane and Coal Chemical Looping Combustion, *Applied Energy*, **157**: 348-357 (2015).

[60] Zhao K., Li L., Zheng A., Huang Z., He F., Shen Y., Zhao Z., Synergistic Improvements in Stability and Performance of the Double Perovskite-Type Oxides $La_{2-x}Sr_xFeCoO_6$ for Chemical Looping Steam Methane Reforming, *Appl. Energy*, **197**: 393-404 (2017).

[61] Zhao K., He F., Huang Z., Wei G., Zheng A., Li H., Zhao Z., Perovskite-Type Oxides $LaFe_{1-x}Co_xO_3$ for Chemical Looping Steam Methane Reforming to Syngas and Hydrogen co-Production, *Appl. Energy*, **168**: 193-203 (2016).